11032 *Inorg. Chem.* **2009**, *48*, 11032–11037
DOI: 10.1021/ic901205c

Inorganic Chemistry
Article

Synthesis and Optical Properties of Guanosine 5′-Monophosphate-Mediated CdS Nanostructures: An Analysis of their Structure, Morphology, and Electronic Properties

Anil Kumar*,†,‡ and Vinit Kumar†

†*Department of Chemistry, and* ‡*Centre of Nanotechnology, Indian Institute of Technology Roorkee, Roorkee - 247667, India*

Received June 23, 2009

The present manuscript reports the synthesis, characterization, and analysis of electronic properties of water-soluble guanosine 5′-monophosphate (GMP)-mediated CdS quantum dots (Q-dots). The morphology, size, and size distribution of these particles have been analyzed by transmission electron microscopy. These particles display the onset of absorption at 2.7 eV and emission at 2.2 eV. In comparison to other monophosphate**s** of RNA (AMP, UMP, and CMP), GMP-mediated CdS exhibits enhanced electronic properties. The participation of different functional groups of GMP in the stabilization of CdS nanoparticles has been analyzed by FTIR and ^{1}H and ^{31}P NMR spectroscopic techniques. Two types of binding sites involving phosphorus centers are indicated by IR and ^{31}P NMR studies. The conversion of CdS Q-dots to nanorods has been monitored by using electron microscopy, steady-state optical and fluorescence measurements, and a fluorescence lifetime system coupled with anisotropy accessories. The observed change in the morphology and electronic behavior of GMP- and RNA-mediated CdS nanostructures is discussed on the basis of their structural difference.

1. Introduction

A large number of biomolecules like proteins, lipids, nucleic acids, antibodies, antigens, and enzymes having nanoscale dimensions constitute the fundamental building blocks of natural systems.[1,2] In these systems, several biological molecules exist as supramolecular aggregates consisting of complex microstructures and are being utilized to develop biological machines in the nanoscale domain for applications in ultrasmall electronics and devices.[3−8] Among different biomolecules, functionalized biopolymers like DNA[9] and RNA[10,11] have lately been employed extensively for templating of nanomaterials. These consist of long-range nanoscale order, which could be tailored to fabricate artificial nanostructures with varied properties. Integration of the functionalized biomolecules to inorganic nanomaterials may generate new materials with enhanced optical, fluorescence, magnetic, and electronic properties and increased photostability.[4,12,13] In recent years, there has been enormous interest in making nanohybrids of quantized semiconductor and biomolecules,[14−16] in efforts to replace the fluorescent organic dyes employed as biomarkers,[17] since semiconductor quantum dots (Q-dots) have several added advantages over organic dyes in regard to their tunable optical and fluorescing properties, increased solubility, and enhanced chemical and photostability. An understanding of the interaction/binding of semiconductor quantum dots with biomolecules through its various functional sites may provide a key to optimizing and controlling the growth needed for the design of new nanostructures.

In previous studies, nucleotide triphosphates have been shown to be the effective ligands for the stabilization of

*To whom correspondence should be addressed. Tel.: +91-1332-285799. Fax: +91-1332-273560. E-mail: anilkfcy@iitr.ernet.in.

(1) Prasad, P. N. *Nanophotonics*; John Wiley & Sons: New Jersey, 2004; Chapter 12, pp 337−353.
(2) Willner, I.; Willner, B.; Katz, E. *Bioelechem* **2007**, *70*, 2–11.
(3) Mann, S. *Angew. Chem., Int. Ed.* **2008**, *47*, 5306–5320.
(4) Niemeyer, C. M. *Angew. Chem., Int. Ed.* **2001**, *40*, 4128–4158.
(5) Gracia-Garibay, M. A. *Nat. Mater.* **2008**, *7*, 431–432.
(6) Sotiropoulou, S.; Sierra-Sastre, Y.; Mark, S. S.; Batt, C. A. *Chem. Mater.* **2008**, *20*, 821–834.
(7) Sanchez, C.; Arribart, H.; Guille, M. M. G. *Nat. Mater.* **2005**, *4*, 277–287.
(8) Johnston, A. P. R.; Zelikin, A. N.; Caruso, F. *Adv. Mater.* **2007**, *19*, 3727–3730.
(9) Storhoff, J. J.; Mirkin, C. A. *Chem. Rev.* **1999**, *99*, 1849–1862.
(10) Feldheim, D. L.; Eaton, B. E. *ACS Nano* **2007**, *1*, 154–159.
(11) Kumar, A.; Kumar, V. *J. Phys. Chem. C* **2008**, *112*, 3633–3640.
(12) Ma, N.; Sargent, E. H.; Kelley, S. O. *J. Mater. Chem.* **2008**, *18*, 954–964.
(13) Whaley, S. R.; English, D. S.; Hu, E. L.; Barbara, P. F.; Belcher, A. M. *Nature*. **2000**, *405*, 665–668.
(14) Dooley, C. J.; Rouge, J.; Ma, N.; Invernale, M.; Kelly, S. O. *J. Mater. Chem.* **2007**, *17*, 1687–1691.
(15) Berti, L.; Burley, G. A. *Nat. Nanotechnol.* **2008**, *3*, 81−87 and references therein.
(16) Green, M.; Symeth-Boyle, D.; Harries, J.; Taylor, R. *Chem. Commun.* **2005**, 4830–4832.
(17) Stephens, D. J.; Allan, V. J. *Science* **2003**, *300*, 82–86.

 Published on Web 11/10/2009

fluorescing CdS nanoparticles;[14,16] it is the monophosphate(s) of nucleotides, which constitute different components of RNA and DNA. In the present work, we have examined nucleotide monophosphates, namely, guanosine 5′-monophosphate (GMP), adenosine 5′-monophosphate (AMP), cytidine 5′-monophosphate (CMP), and uridine 5′-monophosphate (UMP), as templates for the synthesis of CdS nanoparticles and assessed the contribution of each of the components toward electronic properties. We did not come across any extensive studies on these systems in the literature. Among the investigated components, GMP (Figure 1) stabilizes CdS nanostructures effectively and exhibits a more prominent excitonic band, relatively higher fluorescence quantum efficiency, and a longer emission lifetime. Aging of these nanoparticles transforms them to nanorods. A difference in the morphology and electronic behavior of GMP- and RNA-mediated CdS nanostructures is also discussed.

2. Experimental Section

Materials. Cadmium perchlorate, guanosine 5′-monophosphate, adenosine 5′-monophosphate, cytidine 5′-monophosphate, uridine 5′-monophosphate (Sigma); FeS, perchloric acid, and NaOH (Merck) were of analytical grade and were used without any further purification. Nitrogen (99.9% Sigma) was used for deoxygenating the solution during synthesis. All experiments were performed in an aqueous medium.

Equipment. UV−visible absorption and steady-state emission spectra were recorded on a Shimadzu UV-2100S spectrophotometer and Shimadzu RF-5301-PC spectrofluorophotometer, respectively. Electron microscopy and selected area electron diffraction patterns were performed on a digital FEI-TECNAI transmission electron microscope operating at 200 KeV. The size of different nanostructures was determined from their transmission electron microscopy (TEM) micrographs using digital micrograph software. Sample(s) for TEM analysis were prepared by applying a drop of the colloidal solution to a carbon-coated copper grid. The excess solution was then removed after about 2 min with a tissue paper. X-ray diffraction patterns were obtained on a Philips DW 1140/90 X-ray diffractometer using the Cu Kα line (1.5418 A°) of the X-ray source. The ^{1}H and ^{31}P NMR spectra were obtained on a Bruker Avance 500 spectrometer working at 500 MHz. For ^{31}P NMR studies, a 10% solution of H_3PO_4 was used as an external reference. All NMR data were collected in deuterated aqueous solutions. IR spectra in the mid-IR range were recorded on a Thermo Nicolet Nexus FTIR spectrophotometer. The time-resolved fluorescence and fluorescence anisotropy decay measurements were made on a Horiba Jobin Yvon-IBH single-photon counter using the time domain method. NanoLEDs and LDs were used as excitation sources. An iterative reconvolution technique using a multiexponential fitting program was used for the analysis of decay curves.

Synthesis of Nanoparticles. GMP-, AMP-, CMP-, and UMP-stabilized CdS nanopatricles were synthesized by adding varied concentrations of these substrates (0.001−0.015 g/100 mL) and Cd^{2+} (2×10^{-4} mol dm^{-3}) at pH 9.2 followed by the injection of SH^- at room temperature (∼ 20 °C). In all cases, the reaction mixture(s) were purged with nitrogen under continuous stirring for about 15 min prior to the injection of SH^-. Among these, CMP forms a complex with Cd^{2+} and precipitates out, even at its lowest concentration, that is, 0.001 g/100 mL. Thus, it could not become possible to produce CMP-templated CdS. However, UMP-stabilized CdS particles could be produced by employing a relatively much higher concentration of nucleotide (0.025 g/100 mL) and by the slow addition of Cd^{2+} (2×10^{-4} mol dm^{-3}) to the nucleotide solution at 0 °C. All of the samples were purged with nitrogen under continuous stirring for 15 min prior to the injection of SH^- prepared by the acid decomposition of FeS. An increase in the concentration of these solutes blue-shifts both the onset and the exciton absorption. Electronic properties of GMP- and AMP-mediated CdS were optimized by varying the experimental conditions of pH (9.2−10.2) and the concentration of the nucleotide (0.001−0.015 g/100 mL). The best conditions under which the strong excitonic absorption and emission were observed correspond to 0.015 g/100 mL of the nucleotide, $Cd^{2+} = 2 \times 10^{-4}$ mol dm^{-3}, and $HS^- = 1 \times 10^{-4}$ mol dm^{-3} at pH 9.2. Both GMP and AMP produced highly water-soluble CdS nanoparticles.

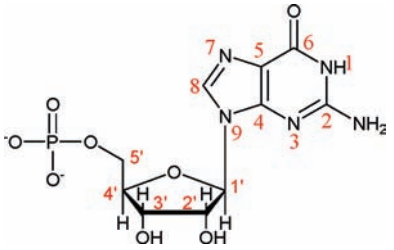

Figure 1. Chemical structure of GMP.

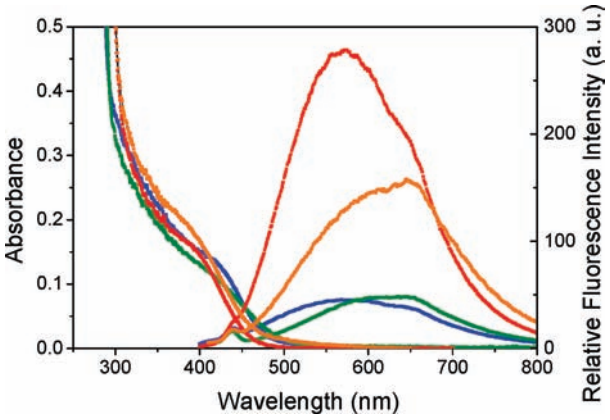

Figure 2. Electronic and emission spectra of CdS-mediated by GMP [fresh (red), aged (orange)], AMP (blue), and UMP (green) (λ_{ex} = 380 nm).

3. Results and Discussion

Results. Optical Properties. For a typical case of GMP, the effect of variation of its concentration (0.001 g/100 mL to 0.015 g/100 mL) on the optical and emission behavior of CdS is shown in Figure S1 (Supporting Information). An increase in the concentration of GMP blue-shifts the onset of absorption and emission maxima from 2.5 to 2.7 eV and 2.0 to 2.2 eV, respectively. A comparison of electronic and emission data of GMP-, AMP-, and UMP-mediated particles demonstrates that, for the latter two systems, the excitonic absorption and emission maxima are slightly red-shifted. The emission band becomes broad, and intensity is reduced to about 40% in each case (Figure 2).

TEM and SAED. Electron micrographs of GMP-, AMP-, and UMP-mediated CdS particles consisted of aggregates of a large number of spherical particles having a size (size distribution) of 5 nm (2−8 nm), 7.5 nm (3−12 nm), and 10 nm (8−15 nm), respectively (Figure 3; Supporting Information, Figure S2). The difference in their size is consistent with their electronic spectral data,

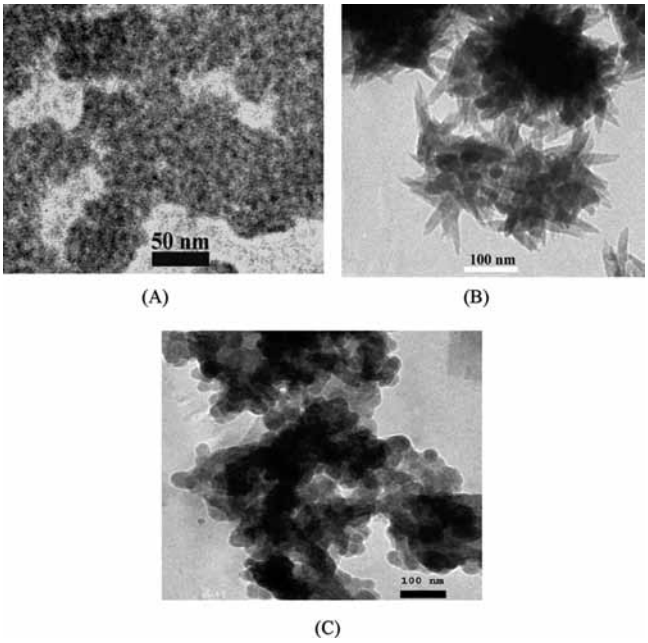

Figure 3. TEM images of fresh (A) and aged (B) GMP-CdS. TEM of GMP−Cd^{2+} (C).

as GMP-stabilized particles depicted the blue-shifted onset of absorption, excitonic peak, and the fluorescence maxima compared to that of AMP- and UMP-mediated particles.

Interestingly, the aging of GMP-mediated Q-CdS for a period of three months exhibits a change in their shape from spherical Q-dots to nanorods with an average length and diameter of 73 nm (64−83 nm) and 21 nm (18−24 nm), respectively, giving an average aspect ratio of about 3.5 (Figure 3). In order to probe the role of excess Cd^{2+} in the observed change in morphology, in a control experiment, the TEM image of GMP was recorded in the presence of excess Cd^{2+}. It produced spherical particles with an average size (size distribution) of 36 nm (24−45 nm). It thus rules out the contribution due to simple interaction of excess Cd^{2+} with GMP in the formation of nanorods. These changes are represented diagrammatically in Scheme 1. The formation of self-assembly was also monitored by recording the optical and emission behavior upon aging. It shifted the excitonic absorption to higher energy with about a 1.3-fold increase in the coefficient of absorption, while the emission peak is red-shifted with about a 1.6-times reduction in the emission intensity (Figure 2).

An analysis of selected area electron diffraction patterns of fresh and aged GMP-stabilized CdS depicts reflections corresponding to (002), (110), (200), (203), (210), and (212) and (101), (102), and (110) planes, respectively, each of which belong to the hexagonal phase of CdS. The hexagonal phase of CdS is also confirmed by XRD patterns of the powder, showing the dominant peak corresponding to the (002) plane reflection (Figure 4).

FTIR. In order to analyze the interaction of Cd^{2+} and CdS nanoparticles with GMP, FTIR spectra of Na_2−GMP, GMP−Cd^{2+}, and GMP−CdS were recorded under identical experimental conditions (Supporting Information, Figure S3 and Table S1). The IR spectrum of Na_2−GMP shows all of its characteristic

Scheme 1

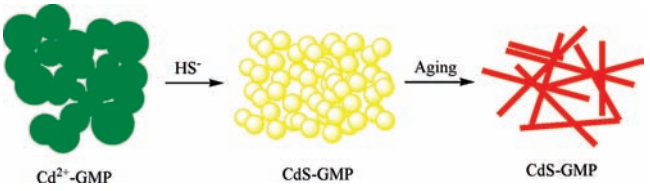

peaks as reported in the literature.[18] The IR spectrum of Cd^{2+}−GMP exhibits binding of Cd^{2+} to GMP through >C=O, $-NH_2$, $-PO_3^{2-}$, and P−O−-5′-sugar, as was indicated by a shift in frequencies due to these groups along with a change in the nature of their bands. The formation of CdS nanoparticles was observed to influence imidazole and pyrimidine ring vibrational frequencies and the group frequencies as was indicated by a change in the nature of bands corresponding to these moieties.

^{1}H and ^{31}P NMR. The nature of interaction of Cd^{2+} and CdS nanoparticles with GMP was further probed by ^{1}H and ^{31}P NMR spectroscopy by recording NMR spectra of pure GMP, GMP−Cd^{2+}, and GMP−CdS prepared under identical conditions of pH. A comparison of chemical shift (δ) values in ^{1}H NMR for H(8) of Cd^{2+}−GMP and GMP−CdS shows a relatively higher resonance absorption frequency by a magnitude of 0.1 ppm and 0.2 ppm, respectively, compared to that of pure GMP (Supporting Information, Figure S4). An examination of ^{31}P NMR spectra of blank Cd^{2+}−GMP and CdS−GMP nanosystems (Figure 5) suggests the presence of two types of phosphorus centers in each case, as was revealed by their resonance absorptions having δ values of 2.53 and 2.01 ppm and 3.68 ppm and 2.46 ppm, whereas the resonance absorbance due to phosphorus in pure GMP exhibited only a single absorption peak at δ of 2.74 ppm. Obviously, among these systems, the formation of CdS nanostructures influences the magnitude of chemical shift more significantly.

Charge Carrier Dynamics. The photophysics of these systems was analyzed by monitoring the relaxation kinetics of charge carriers under varied experimental conditions. Under all conditions, the fluorescence decay curves followed three-exponential kinetics. Major components contributing to the fluorescence decay correspond to subnanosecond (80.3%) and nanosecond (12.3%) time domains (Table 1). The component corresponding to a longer time constant has a relatively small contribution of about 7.4% only and is consistent with a relatively lower steady-state quantum efficiency of fluorescence (~0.01). Upon the aging of these particles for three months, the percentage emission corresponding to the subnanosecond time domain is slightly increased, whereas for components 2 and 3, the emission percentage is slightly decreased. These observations are supported by a reduction in the intensity of emission spectra accompanied with a decrease in the average lifetime, due to these particles, from 48 to 43 ns upon aging (Figure 6). These particles exhibit relatively higher stability and

(18) Nafisi, Sh.; Mohajerani, N.; Hadijakhoondi, A.; Monajemi, M.; Garib, F. *J. Mol. Str.* **2001**, *562*, 35–43.

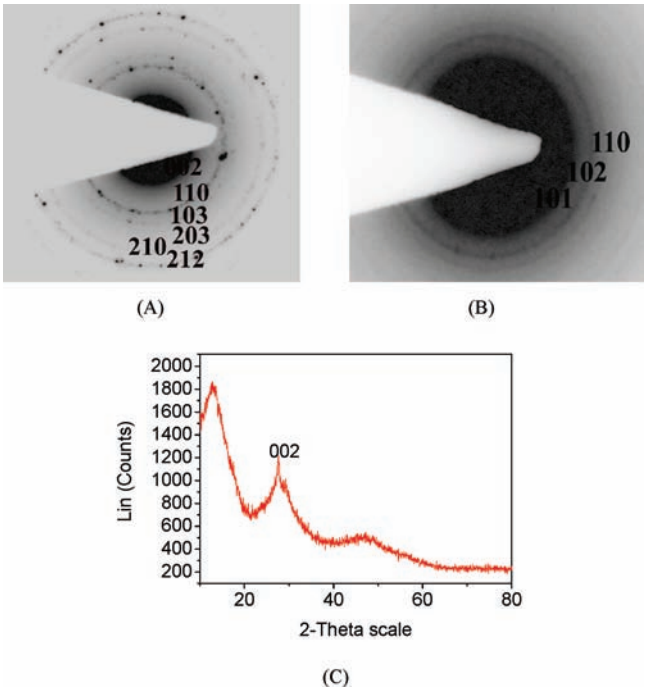

Figure 4. SAED of fresh (A) and aged (B) GMP−CdS. XRD patterns of GMP-stabilized CdS nanoparticles (C).

fluorescence intensity as compared to those reported previously for such system(s).[14,15]

Fluorescence Anisotropy. The value of fluorescence anisotropy (r) for fresh GMP-stabilized CdS comes out to about 0.05, which increased to 0.25 upon aging (Supporting Information, Figure S5). An increase in the value of anisotropy suggests aged nanostructures to be partially polarized by attaining a particular orientation. A change in anisotropy is also consistent with the observation made by electron microscopy, which demonstrated the transformation of the Q-dots to nanorods upon aging.

Discussion. The stabilization of CdS nanohybrids by GMP can be ascribed by the binding of its different functional sites of pyrimidine, purine, and phosphate sugar to the surface of CdS (Figures S3 and S4, Supporting Information). The [GMP] affects the extent of binding of CdS through its functional groups and is thus understood to control the optical and photophysical properties of these nanostructures (Figures S1A and S1B, Supporting Information). The concentration-dependent changes in the properties are consistent with these particles to be produced in the confined region, as is also supported by the electron microscopy data (Figure 3).

Both IR and NMR spectroscopic data on the GMP−CdS nanohybrid suggest the presence of two binding sites involving phosphorus centers. In the IR spectrum of Cd^{2+}−GMP, an increase in the antisymmetric stretching frequency of PO_3^{2-} and a slight decrease in the P−O stretching frequency due to P−O−5′-sugar are understood to occur due to their coordination with Cd^{2+}. On the contrary, upon the formation of the CdS−GMP nanohybrid, no appreciable change in the antisymmetric stretching frequency of PO_3^{2-} is recorded, but there was an additional decrease in the P−O stretching frequency due to P−O−5′-sugar (Table S1, Supporting Information). These observations suggest that Cd^{2+} mainly interacts with the anionic oxygen of PO_3^{2-} and CdS interacts through ethereal oxygen of P−O−5′-sugar, respectively. Whereas in ^{31}P NMR spectra of Cd^{2+}−GMP and CdS−GMP, resonance absorptions at two positions were recorded corresponding to the phosphorus center unlike to the single absorption peak with pure GMP (Figure 5). These data further demonstrate that in case of CdS−GMP the observed two peaks are more prominent, and the difference in the values of the chemical shift was fairly high compared to that of Cd^{2+}−GMP. Thus, IR and NMR studies clearly indicate that Cd^{2+} gets bound mainly through PO_3^{2-} with a partial interaction with P−O−5′-sugar, and on the other hand, CdS interacts prominently through P−O−5′-sugar.

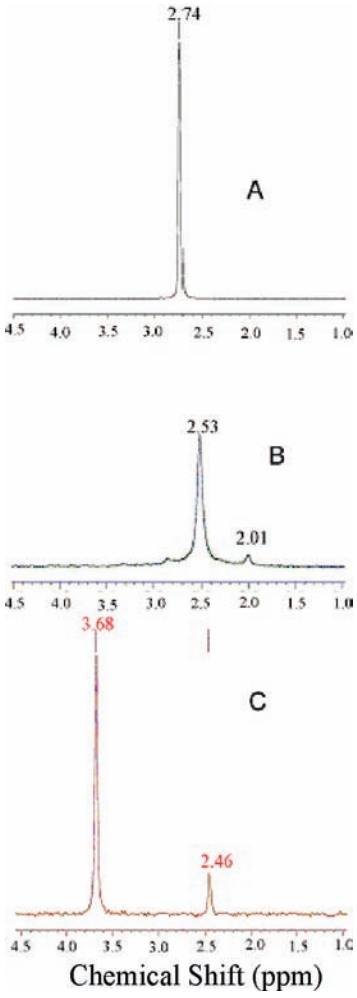

Figure 5. ^{31}P NMR spectra of pure GMP (A), Cd^{2+}−GMP (B), and CdS−GMP (C).

It may be further argued that the electron density on the oxygen of the P═O bond will be higher compared to that of ether oxygen in P−O−5′-sugar, which should cause more interaction of Cd^{2+} through the oxygen of the P═O bond. But, the observed absence of interaction of CdS with the oxygen of P═O though can be understood because of its planar geometry with the fixed structure compared to more flexibility in its binding through the ether oxygen of P−O−5′-sugar, having single bond connections with P and (phosphate) esters.

Table 1. Lifetimes of GMP-Capped CdS (λ_{ex} 375 nm; λ_{em} 570 nm)

	component 1		component 2		component 3			
GMP−CdS	τ_1 (ns)	emission %	τ_2 (ns)	emission %	τ_3 (ns)	emission %	$<\tau>$ (ns)	χ^2
Q-dot	6.4 (0.0319)	12.3	62.3 (0.0191)	7.4	0.8 (0.207)	80.3	48	1.0
nanorods	9.1 (0.0503)	11.7	60.0 (0.0304)	7.0	1.1 (0.351)	81.3	43	1.1

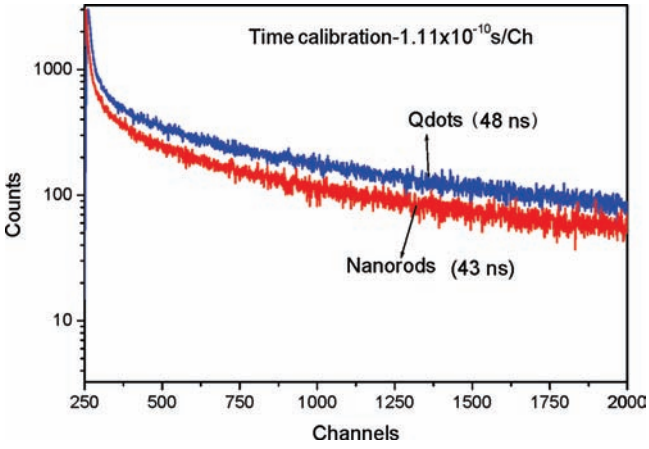

Figure 6. Decay curves of GMP-capped CdS Q-dots and nanorods [λ_{ex} 375 nm; λ_{em} 570 nm].

A transformation in the shape of these nanostructures, that is, from quantum dots to nanorods, can be understood by their reorganization with aging over a period of three months. In fact, CdS nanohybrids functionalized by GMP might interact with other similar nanohybrids as well as with the free GMP available in solution. It might occur either by the binding of two Q-dots through Cd^{2+} to the anionic oxygen of PO_3^{2-} and subsequent oriented attachment of such units or with the free GMP through H-bonding (Scheme 2).[19] Increased oscillator strength upon aging supports the quantum confinement in two dimensions of nanorods.

GMP is also known to undergo H-bonding interactions to form G- quartet or G- nanowires.[20,21] Its formation though requires about a 3 orders of magnitude higher concentration of GMP[22,23] compared to that employed in the present work. Further, the formation of G-quartet is associated with the broadening of the H(8) line in the ^{1}H NMR spectrum of GMP.[22,23] Since the [GMP] employed in the present work is fairly low and ^{1}H NMR spectra of pure GMP, GMP−Cd^{2+}, and GMP−CdS demonstrate the absence of the broadening of the H(8) line, it evidently rules out the presence of any dynamic equilibrium involving GMP-mediated CdS quantum dots transforming into templated G-quartet or G-nanowire. A varied extent of H-bonding interactions among CdS-GMP nanostructures might have contributed to the relatively large size distribution observed in TEM.

It may be pointed out that both the optical and fluorescence behavior of GMP, AMP, and UMP in terms

Scheme 2

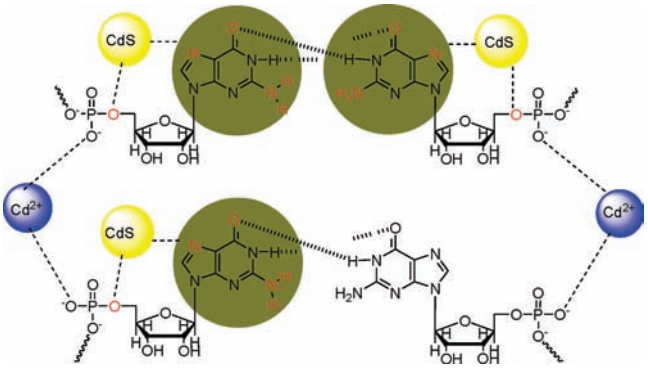

of the onset of absorption, excitonic band, and emission maxima are fairly different from those of GTP, ATP, and UTP,[14,16] suggesting the significance of the number of phosphate group(s) attached to these ligands. Green et al.[16] have also reported the possibility of binding all three phosphate groups and the $-NH_2$ group of ATP/GTP to the surface of CdS particles. For GTP-stabilized CdS nanoparticles, Dooley et al.[14] have reported the interaction of N(7) and phosphate groups of GTP with the CdS surface. Whereas in the present work the coordination of CdS through N(7) of pyrimidine, >C=O and $-NH_2$ of purine and P−O−5′-sugar have been identified, and excess Cd^{2+} is observed to link two such building blocks through the PO_3^{2-} of sugar, which contributed to the passivation of CdS differently in the latter case. Further, the optical properties of CdS nanoparticles capped by GMP, AMP, and UMP reveal them to be markedly different compared to RNA-stabilized Q-CdS nanoparticles, as the latter system demonstrates it to have relatively blue-shifted excitonic absorption (3.3 eV) and emission (2.34 eV) bands.[11] In addition, the aging of RNA-mediated nanoparticles resulted in the formation of a network of nanorods with increased emission intensity and lifetimes of charge carriers. A difference in morphology and electronic behavior in the two cases may be ascribed mainly to the structural difference of RNA with GMP (Figure 1). RNA is a long unbranched polymer containing ribose sugar units with 2′-OH, whereas GMP is a monomeric species containing hydroxyl groups at the 2′ and 3′ positions. Unlike RNA, none of the −OH groups of GMP binds to CdS. Evidently, in the latter case, a difference in specific binding causes the passivation of the surface of CdS differently. These observations clearly manifest the cooperative effect of different components of RNA toward the electronic properties for RNA-mediated particles in contrast to its individual components, the monophosphates.

4. Conclusions

In summary, GMP effectively mediates the synthesis of CdS nanohybrids by coordinating through the N(7) of

(19) Wu, G.; Kwan, I. C. M. *J. Am. Chem. Soc.* **2009**, *131*, 3180–3182.
(20) Davis, J. T. *Angew. Chem., Int. Ed.* **2004**, *42*, 668–698.
(21) Kunstelj, K.; Federiconi, F.; Spindler, L.; Drevenšek-Olenik, I. *Colloid Surf., B* **2007**, *59*, 120–127.
(22) Pinnavaia, T. J.; Miles, H. T.; Becker, E. D. *J. Am. Chem. Soc.* **1975**, *97*, 7198–7200.
(23) Pinnavaia, T. J.; Marshall, C. L.; Mettler, C. M.; Fisk, C. L.; Miles, H. T.; Becker, E. D. *J. Am. Chem. Soc.* **1978**, *100*, 3625–3627.

pyrimidine: the >C═O and $-NH_2$ of purine and P−O−5′-sugar. Transformation of their morphology from spherical Q-dots to nanorods upon aging is understood to propagate by the binding of Cd^{2+} through PO_3^{2-} of two CdS−GMP Q-dots followed by oriented attachment of various such units through H-bonding. Selective binding of nanoparticles to different sites of biomolecule(s) thus provides a means to control the morphology and optical properties of nanohybrids. Synthesis of such nanohybrids provides a method to fabricate biomolecule(s) templated nanostructures with tunable optical and electronic properties.

Acknowledgment. The financial support of CSIR, New Delhi is gratefully acknowledged for undertaking this work. V.K. acknowledges CSIR, New Delhi for the award of SRF. Thanks are also due to the Head, IIC, IITR, Roorkee for providing us the facilities of NMR, TEM, FESEM, XRD, and single photon counter.

Supporting Information Available: Electronic and emission spectra; TEM, ^{1}H NMR, FTIR spectra and spectral data; fluorescence anisotropy. This material is available free of charge via the Internet at http://pubs.acs.org.